Iraqi Journal of Scientific and Industrial Research
Volume 1, Issue (4), October-December 2022, pp. 114-121

# Modification of Raman LIDAR System for Temperature and Water Vapor Measurements in Atmosphere Layers

Mehradad KABRAL

*Radio Communications Research Unit, Ravindra Kumar Institute of Technology, Delhi, INDIA*

**Abstract**
In this work, developing a UV Raman LIDAR system to be used for measuring water vapour and temperature profiles within the troposphere. LIDAR provides a continuous remote sensing method for the simultaneous measurement of temperature and humidity profiles in the troposphere. This enables continuous monitoring of the radio refractivity profile with good time and height resolution, which is of great benefit in radiowave propagation studies. The system is designed to be used by day and night. The main benefit of this technique over the more traditional use of radiosonde ascents is in being able to continuously monitor atmospheric conditions, a capability of great benefit in the modelling of radiowave propagation.

***Keywords***: LIDAR, Troposphere region, Radio refractivity, Temperature profile

**Received:** 2 August 2021; **Revised:** 3 October 2021; **Accepted:** 10 October 2021; **Published:** 1 January 2022

## 1. Introduction

The theory of the technique is described. The development of the experimental hardware has presented many technical challenges, which are discussed, together with the lessons learned. A selection of measurements is presented, highlighting the capabilities of the system in radio refractivity measurements.

The radio refractivity, *N*, defined as (refractive index-1) x$10^6$, at a point in the atmosphere can be expressed as [1]

$$N = \frac{77.6P}{T}\left(1+\frac{4810p_{wv}}{T}\right) \quad (1)$$

where *P* is the atmospheric pressure (mbar), *T* is the temperature (K) and $p_{wv}$ is the partial pressure of water vapour (mbar). *N* is dimensionless but is commonly referred to in *N*-units

By determining temperature and water vapour volume mixing ratio (WVMR) profiles as a function of height, the radio refractivity profile can be deduced. *P* can be measured at the surface and its height dependence deduced using atmospheric density models, if no other source of pressure profiles, such as nearby radiosonde releases, is available.

The gradient of the radio refractivity with altitude gives important information on the paths over which radio waves are propagated. For this purpose it is useful to convert to the quantity of modified radio refractivity, *M*, also a dimensionless quantity, defined as

$$M = N + 157z \quad (2)$$

where *z* is altitude in km [2]

For the majority of time dM/dz>0, but in cases where it is less than zero a condition known as ducting occurs and due to downward curvature of transmitted radiation it is possible for radiowaves to propagate to sites far beyond the horizon [2]. Ducting conditions exist for 5-10% of the time in Northern Europe [2]. Two classes of ducts occur: surface and elevated. Surface ducts occur at or very close to the earth's surface. They are common over bodies of water due to the high levels of water vapour immediately above the surface. Elevated ducts occur at higher levels, typically up to 2 km. The LIDAR system described here is capable of detecting elevated ducts, as in common with most ground-based LIDAR systems, it cannot make measurements down to ground level.

 

Figure (1) shows the extent of an elevated duct for conditions where a negative gradient of *M* occurs.

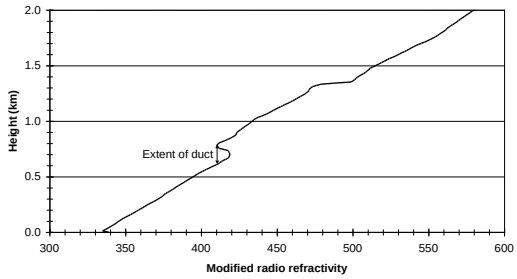


**Fig. (1) Example of the extent of a radio duct from modified radio refractivity measurements.**

Raman scattering is an inelastic quantum mechanical scattering process. When light is incident on a molecule, most of it is elastically scattered, resulting in no shift in wavelength, but a small proportion of the radiation undergoes an inelastic interaction with the molecule in which its wavelength is either increased or decreased compared to the incident wavelength. A wide range of energy changes are possible, but the shift in energy or wavelength is quantised and is a characteristic of the scattering molecule. The interaction between the incoming radiation and the molecule can be either with the vibrational or rotational energy levels of the molecule. Since the vibrational energy levels are more widely spaced than the rotational levels, a change in the vibrational energy of the molecule causes a larger change in wavelength than a change in the rotational energy. The resulting spectrum of Raman scattered radiation consists of more widely spaced bands due to vibrational energy changes, each comprising a set of individual lines due to rotational energy changes.

The water vapour partial pressure is deduced from the ratio of the signal in the first vibrational band of water vapour to that in the same band of molecular nitrogen, $P(z)$. These bands correspond to wavelengths of 407.7, 386.7 nm respectively for incident radiation of 354.7 nm. Since these wavelengths are well separated, it is possible to measure the signal at each scattered wavelength independently. The water vapour partial pressure is related to the WVMR, the fraction of water vapour in the air by number density. The WVMR as a function of height, $x_{wv}(z)$, is given by [3]

$$x_{wv}(z) = KP(z)\frac{T_n(z)d\sigma_n(\pi)/d\Omega}{T_{wv}(z)d\sigma_{wv}(\pi)/d\Omega} \qquad (3)$$

where the subscripts *wv* and *n* refer to water vapour and nitrogen respectively, $K$ is a constant of the LIDAR system relating to the relative sensitivities of the two measurement channels, $T(z)$ is the transmittance of the atmosphere for both the outgoing and returning radiation to height $z$ and $d\square(\square)/d\square$ is the differential back-scattering cross section for Raman scattering of that species

The calibration constant $K$ is determined either by laboratory methods in conjunction with Eq. (3) or by comparison of the measured signal ratio with radiosonde ascents [4,5]. Comparison with routine radiosonde releases from Larkhill, approximately 30 km to the west of Chilbolton, has been used to produce all calibrations used in this work. $T(z)$ for molecular scattering can be calculated by using Rayleigh scattering theory and a standard model for the atmospheric number density as a function of height. The transmittance for aerosol scattering can be calculated either using Raman scattering measurements [6] or a model [7]. A further calibration method which we have been assessing is the use of measurements of integrated water vapour data from the microwave radiometers at Chilbolton, a method which has recently been implemented for the LIDAR measurements at the ARM site in Oklahoma [8]. This approach looks promising, as it has the advantage of being a continuous operation system and is located at the same site. The LIDAR water vapour profiles must be integrated to make a comparison, and there is sometimes significant amounts of water vapour at altitudes greater than can be detected using LIDAR, so some care must be taken in using this method.

The temperature is deduced from the ratio of the signals at 353.0 nm and 353.9 nm in the rotational Raman bands of oxygen and nitrogen. Rotational lines such as these are close to the incident wavelength, which necessitates high rejection filtering of each signal from the much stronger elastically scattered signal. There is also considerable overlap between the two rotational bands, so that the contributions from the individual lines in each band must be modelled in order to extract temperature information. Previous experiments [9,10] have used green radiation at 532 nm, which results in slightly greater spacing of the signals but presents a greater eye hazard.

 

The ratio of the intensity measured in each channel $R(T)$ is given by [9]

$$R(T) = \frac{\sum_i x_i \sum_j P_{ij}(T) N_{ij}}{\sum_i x_i \sum_j P_{ij}(T) F_{ij}} \quad (4)$$

where subscript $i$ refers to each gas (nitrogen and oxygen in this case), $j$ refers to each line in the rotational Raman spectrum for that gas, $x$ is the volume mixing ratio, $P_{ij}(T)$ is the power backscattered into that line and $N_ij$ and $F_{ij}$ are the responses of the receiving optics (filters and detectors) in the near and far bands to the laser line, respectively

Since the wavelengths of the lines are very close to the laser wavelength, it is not necessary to correct for the difference in atmospheric transmittance between the lines.

Temperature measurements are calibrated by either laboratory methods in conjunction with Eq. (4) or by comparison of the measured signal ratio with radiosonde ascents. Software has been developed to perform the quantum mechanics calculations necessary to derive the expected signal ratio as a function of temperature for our system [11]. Figure (2) shows the calculated ratio of signals at 353.0 nm to 353.9nm for our filters. Unlike the water vapour measurements, the temperature is not directly proportional to the measured signal ratio. The calculated ratio is very sensitive to filter transmission and the values of scattering cross-sections used, so that the uncertainties in these values limit the uncertainty which can be achieved in the calibration of the temperature measurements if the laboratory method is used.

The most commonly used method for the measurement of temperature and humidity profiles is the use of radiosondes. The main benefit of LIDAR over radiosondes is that measurements can be made continuously. Another substantial advantage is that the direction of the measurements is well known, whereas the path of a radiosonde is affected by the wind, which often varies with height. Disadvantages of LIDAR are that it is a more complex technique than the use of radiosondes, both in its experimental equipment and the measurement calibration process described above, and it cannot operate through dense cloud.

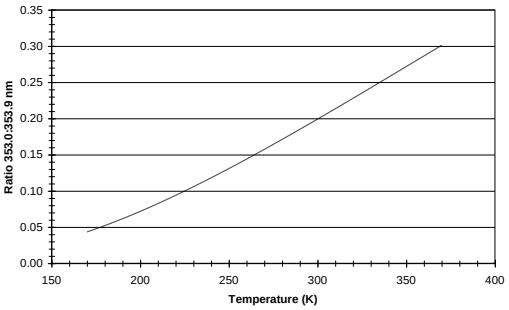


**Fig. (2) Calculated ratio of Raman temperature signals as a function of temperature, for our filters**

## 2. Experimental hardware

The experimental equipment can be divided into three subsystems: transmission optics, receiver optics and data acquisition hardware/software, which are described separately.

The laser used for the project is a Continuum PL9050 series Nd:YAG laser. This type of laser produces infrared radiation, but by the use of frequency doubling and tripling crystals, it produces an ultraviolet beam with a wavelength of 354.7 nm. The laser parameters are shown below.

| | |
|---|---|
| Pulse energy (UV) | 0.35 J |
| Pulse duration | 7 ns |
| Pulse repetition frequency (PRF) | 50 Hz |
| Average power | 17.5 W |
| Beam diameter | 9 mm |
| Beam divergence | 0.5 mrad |
| (0.1 mrad after beam expander) | |

These parameters make the laser one of the most powerful commercially available of its type. A laser of this power was chosen for the project in order to allow Raman LIDAR measurements during daylight hours, when solar radiation is also present at the same wavelengths. In addition, the short pulse duration maintains good height resolution in the measurements, giving an ultimate limit in resolution of approximately 1 m. The use of a UV beam was chosen because it presents much less of an eye hazard than either the green (frequency doubled) or infrared options. In addition, the LIDAR scattering cross-sections are higher at UV wavelengths and the photomultiplier detectors used are more sensitive.

 

During the project there have been some significant difficulties with the laser, which in one case necessitated its return to the suppliers for repairs and modifications. However, operation is now more reliable. Some operational difficulties and frequent maintenance are to be expected when using a laser of this power. Compared with other types of laser which can be used for this work, the Nd:YAG laser is relatively simple and reliable to operate.

From the laser, the beam is transmitted to a beam expander, which expands its diameter to approximately 100mm and reduces its divergence to approximately 0.1mrad. Expansion of the beam greatly improves its eye safety before it is transmitted to the atmosphere, such that a few seconds of accidental exposure will not cause injury. It also reduces the beam divergence, which is necessary for making measurements at higher altitudes. Since the performance of the beam expander is critically dependent on the quality of its optics and their separation, it was custom-built by well-established expertise in the production of such items. Apart from one incidence of beam damage to one of the mirrors in the beam expander, it has performed very reliably and is very beneficial in removing the need for any time-consuming adjustments which would otherwise be necessary to maintain low beam divergence.

After the beam has been expanded it is transmitted vertically into the atmosphere by means of a 45° mirror mounted at the top of the telescope framework.

Before the beam expander, 1-2% of the beam is split off, transmitted to a monitoring system and split again. One part goes to a white macor screen, which fluoresces under UV irradiation. The screen is viewed by a camera, which allows remote continuous monitoring of beam quality. The second part goes to a laser power meter to provide continuous monitoring of beam power. The beam power readings are interfaced to the data acquisition system and saved in each data file. This monitoring system has proved very useful in monitoring laser performance, since during LIDAR operation the operator is not in the same room as the laser. In any case monitoring of the full beam would require interruptions of measurements and be considerably more hazardous due to the high beam power.

Figure (3) shows a diagram of the layout of the transmitter and receiver optics.

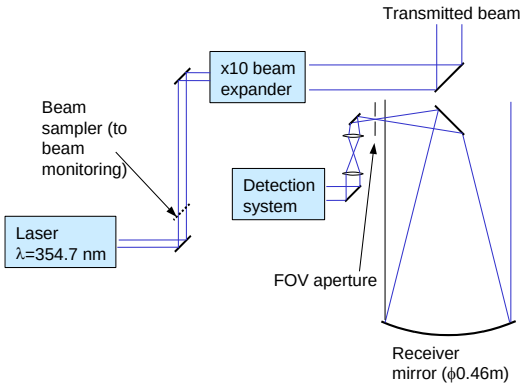


**Fig. (3) Layout of the transmitter and receiver optics**

The returned signals are collected by a telescope with a Newtonian layout, coaxial with the transmitted beam. The telescope framework was built in-house. The variable field-of-view (FOV) aperture at the prime focus of the main mirror is used to adjust the FOV of the measurements. This in turn determines the degree of overlap of the receiver FOV with the transmitted beam. The minimum FOV is 0.5 mrad and for daytime measurements it is beneficial to keep the FOV close to its minimum in order to reduce the detected sky background. Under these conditions useful measurements can be made from a height of approximately 150m upwards. After the aperture, a series of lenses is used to produce a parallel beam which is transmitted to an optical table on which the detectors are mounted. Before detection, the beam is split into five parts, as shown in Fig. (4). This provides beams for the four channels necessary for the Raman scattering measurements, with the fifth beam used to monitor elastic scattering, which provides information on aerosols and clouds. The optics used to perform the splitting were chosen to split the beam efficiently, as signal magnitudes differ between the scattering wavelengths. The wavelength filtering is provided by custom made interference filters produced by Barr Associates (USA), a widely used supplier of custom-made LIDAR filters. In particular, the filters used for the temperature measurements have very strict centre wavelength and elastic scattering rejection requirements as they are so close to the laser

 

wavelength. The Raman filters have been found to be adequate for the requirements of this experiment, although some breakthrough of elastic cloud returns is seen from thick clouds.

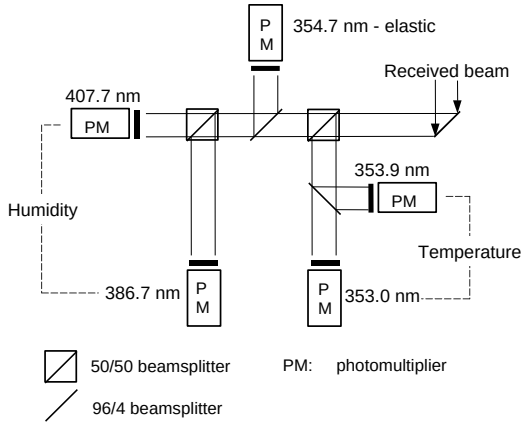


**Fig. (4) Diagram of LIDAR detection optics**

The performance of the detectors is critical in this application and photomultiplier tubes are widely used in LIDAR measurements. They must have a rapid response in order to accurately reproduce the rapidly changing LIDAR return. For the daytime Raman scattering measurements they must be able to measure this signal in the presence of a sky background which in the case of the water vapour measurements is larger than the LIDAR signal. They must also have a large dynamic range. The performance of the existing Electron Tubes photomultiplier detectors has been found to be adequate. Some work has been done in investigating the performance of newer tubes which should be better suited to LIDAR measurements of this type, but this did not indicate an immediate need to change the tube type. Preamplifiers have been developed in-house to optimise the intensity and time response of the signals from the photomultiplier detectors. They are operating well.

A calibration system has been built for the receiver detectors, with the aim of being able to calibrate the ratios of signals received to produce absolute temperature and WVMR values without the need for comparison with other remote sensing systems. It consists of a standard tungsten halogen lamp of known irradiance as a function of wavelength, which can be transmitted as a parallel beam into the receiver optics system to measure the relative responses of the channels. The system currently produces calibration factors which agree with those obtained from Larkhill radiosonde ascents to within 10-15%. Given that the two calibration methods are very different, and that the radiosondes are not released from the same location as the LIDAR, this represents a good agreement. The white light system therefore provides a convenient method of monitoring the LIDAR calibration, although radiosonde ascents should also be included in the calibration scheme.

The detector signals are measured as analog voltages. The data acquisition system comprises three 8-bit Gage CS225 analog data acquisition cards installed in three PCs, each capable of acquiring data at 25 MHz (corresponding to 6 m height resolution) on two channels simultaneously. The code used to collect data from each card is written in C, with LabView software used to collate the data from the cards, control the timing of the measurements and save the data. Information is also stored from the low power meter and a temperature/humidity sensor in the LIDAR room. All the data acquisition software was written in-house. The data acquisition system works well. Some upgrades are desirable however to improve the quality of the data. 12-bit cards are now available with the same acquisition rate and the use of these would give a significant improvement in data quality. For night time measurements, when there is no sky background in the Raman measurements, it would be preferential to use a pulse counting method for measuring the detector signals, rather than analog voltage measurements. This method has the benefit of greater sensitivity at low light levels.

## 3. Results and discussion

### 3.1 Water vapour

Figure (5) shows WVMR profiles recorded during part of 15/11/01. They are calibrated by comparison with Larkhill radiosonde ascents on several days within a period of around 2 weeks from the measurements. Calibrations from these days show good agreement. As can be seen, the profile shows a relatively complex structure in the lowest 2km. Water vapour profiles vary greatly from day to day, but in general, a monotonic fall in water vapour with height is a common form. The profile may also be fairly flat through the boundary layer, which is well mixed and typically 1-2 km thick at Chilbolton

 

(lower thicknesses being in winter). It then falls fairly rapidly above this height. So the profile from 15/11/01 is unusual. Up to an altitude of around 1 km the water vapour content is relatively high, then it falls rapidly and there is a dry layer. Until around 15:00 a further moist layer is resolved, followed by a further dry layer and a more extensive moist layer. By around 15:00 the two dry layers merged. From 16:00 a further very moist layer developed at around 0.5-0.7 km. Eventually clouds formed in this layer. Their presence can be deduced from the increased noise in the profile above that height, towards the end of the plot. Measurements ended at approximately 16:30 due to this cloud. Otherwise there was no cloud detected at the altitudes shown in the plot.

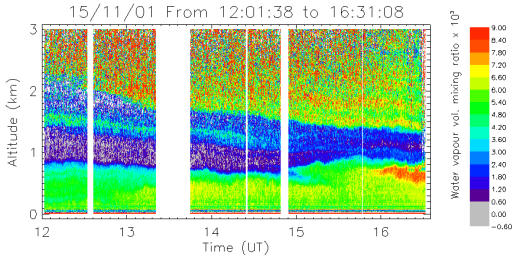


**Fig. (5) Water vapour profiles on 15/11/01. Data averaged over 20s and 6 m height interval**

During daytime measurements, solar radiation is also detected in both the water vapour and nitrogen channels. It is much more dominant in the water vapour channel. This increases the noise in the WVMR measurements, which can be seen by looking at the higher levels in the plot. By 15:30, the noise levels can be seen to be falling, and this trend continues (sunset was at 16:18 UT).

Figure (6) shows individual vertical profiles from these data at 12:05 and 15:00. They are compared with Larkhill radiosonde ascents at the closest available time. As can be seen there is good agreement in the profiles, given their temporal and geographical separation. The LIDAR profiles can be seen to become noisier with height, as the actual measured returns become smaller. They are also noisy in the first approximately 0.1 km, where the returns are again small due to a small degree of overlap between the transmitted beam and the receiver field of view.

Using Eq. (1) and (2) the water vapour profile can be used to determine the gradient of modified radio refractivity, and hence the position of any ducts identified. Qualitatively, a duct may be present if there is a sufficiently large negative gradient in the water vapour content with height. The atmospheric pressure and temperature as a function of height are also needed for the calculations. In the following examples of ducts, these values were determined from Larkhill radiosonde data. In future, LIDAR temperature measurements (discussed later in this section) should be available, and pressure profiles can be calculated from the surface pressure and modelled information on atmospheric density profiles. Hence, radiosonde data would not be necessary. Figure (7) shows the modified radio refractivity gradient derived from the 15/11/01 water vapour profiles. A duct was detected, which persisted through the measurement period.

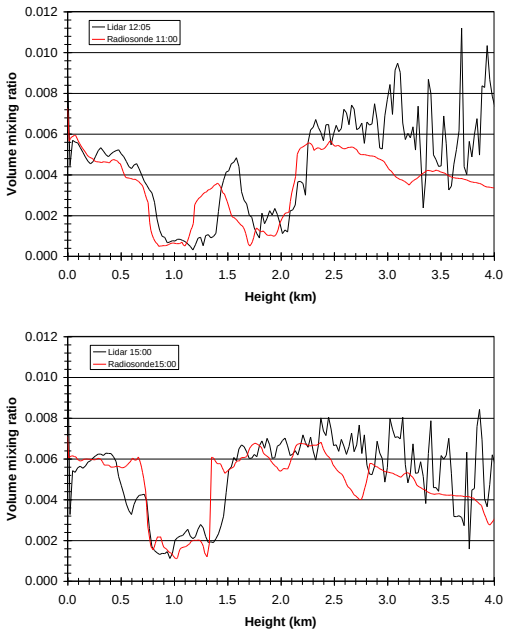


**Fig. (6) Comparison of LIDAR profiles and radiosonde ascents on 15/11/01. LIDAR data averaged over 5 minutes and 24 m height intervals**

Figure (8) shows water vapour profiles recorded on 14/02/02. Skies were mainly clear, although a few cumulus clouds were detected at around 1 km between 14:00 and 16:00, causing the intermittent increased noise in the ratio from heights above the cloud. The air was relatively dry on this day, and the water vapour mainly confined to altitudes less than around 2 km, with very dry air above. The profiles did not show layering structure such as was seen on

 

15/11/01. The two plots show the reduction in noise achieved by averaging data recorded over a period of 5 minutes. They also show the large reduction in noise which occurs as the sky becomes dark. Sunset was at 17:19 UT, so by 18:00 the sky appeared completely dark. Up to around 1.5 km, the visual effect of noise due to the sky background is not large, as the LIDAR returns are also relatively large here. At higher altitudes, especially with the low amounts of water vapour seen on this day, the reduction of noise after dark greatly improves the signal:noise ratio of the system. For radio refractivity measurements, these limitations are acceptable, as it is at lower levels, where amounts of water vapour are generally higher, where the water vapour contribution to the radio refractivity has the most significant effects on the overall value and its gradient.

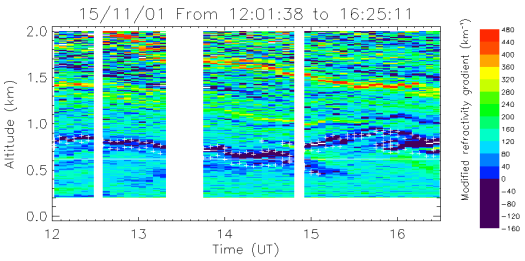


**Fig. (7) Gradient of modified radio refractivity profiles on 15/11/01. Data averaged over 5 minutes and 6 m height intervals. The extent of the duct is identified by white crosses**

As the LIDAR measurements to date have only sampled a very small spread of atmospheric conditions, it is not possible to draw conclusions about the frequency of occurrence of ducts at Chilbolton. Most of the measurements made so far do not show their presence.

### 3.2 Temperature

Measurements using the two temperature channels are being made simultaneously with water vapour measurements. However, they are not as advanced as the water vapour measurements and are not yet producing calibrated temperature values. The filters have been found to be adequate, with rejection of the elastic return of $2x10^{-5}$ for the 353.0 nm filter and $3x10^{-4}$ for the 353.9 nm filter. In the longer term however, filters with a higher rejection may be desirable.

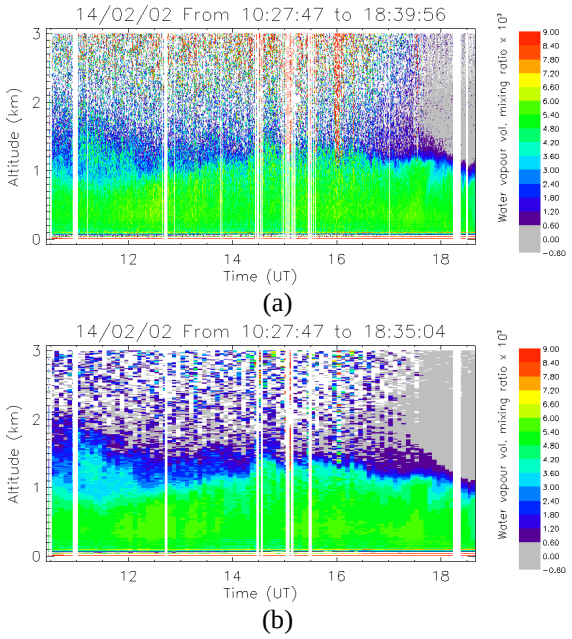


**Fig. (8) Water vapour profiles on 14/02/02 (a) Data averaged over 20 seconds and 6 m height intervals. (b) Data averaged over 5 minutes and 6 m height intervals**

Figure (9) shows the LIDAR temperature measurement as a ratio of the signals in the two temperature channels, together with the temperature profile measured by the Larkhill radiosonde, both recorded on 24/04/02 at 12:00. Figure (2) shows a relationship which is close to linear with an offset between measured ratio and temperature over small temperature ranges. The LIDAR signal ratio appears to show the expected features, such as the inversion at around 1.7 km and possibly that at around 0.6 km also. However the LIDAR signal ratio appears lower than expected in the lowest approximately 1 km, an effect that has been seen on other days also. The dotted line shows an estimate of the ratio which would be expected, based on the radiosonde profile. Hence it appears that the LIDAR temperature measurements do reflect the actual temperature profile, but that some more work is needed to remove the remaining discrepancies. It is not certain what is causing the discrepancies. Two possibilities are that either the two channels see a different degree of overlap between the transmitted beam and the receiver FOV due to small differences in optical alignment, or that the two detectors are showing slightly different response times. A typical temperature profile shows much smaller variations on the absolute temperature scale than the water vapour profile,

 

making it more important to be able to extract relatively smaller features from the signal ratio when making temperature measurements.

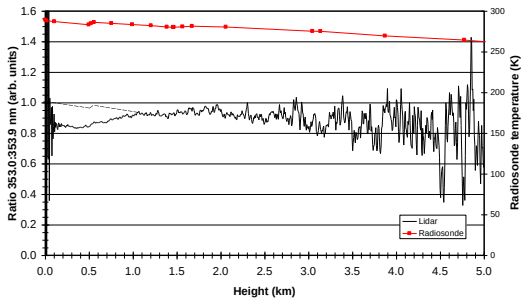


**Fig. (9) LIDAR temperature (as a signal ratio), compared with a radiosonde measurement at 12:00 on 24/04/02. Data averaged over 5 minutes and 6 m height intervals**

Ideally, it is desirable to measure radio refractivity to an uncertainty of ±1 *N*-unit. At typical conditions for ground level, this requires an uncertainty of less than approximately ±0.8K in the temperature measurement or approximately ±0.2 mbar in water vapour partial pressure. These are both quite difficult targets for such a remote sensing technique and there are several sources of uncertainty in the LIDAR measurements which make a total uncertainty of ±1 *N*-unit difficult to achieve. By comparison, the radiosondes commonly used for routine releases at present quote uncertainties of ±0.2K in temperature measurements (at low altitudes) and ±3%□RH for relative humidity measurements, which convert to <±0.5 *N*-unit, ±(2-3) *N*-unit uncertainties respectively. In the LIDAR measurements there will be contributions from both systematic and random uncertainties. Random uncertainties will be reduced by increasing the integration time for profiles or reducing the height resolution. The use of temporal and spatial integration will be determined by the purpose of a particular measurement sequence. Systematic sources of uncertainty, for example those resulting from errors in calibration of the measurements, also contribute. Systematic uncertainties may be less critical, as radio refractivity modelling is often concerned with spatial or temporal variations in refractivity and so will be less affected by systematic uncertainties.

## 4. Conclusions

A Raman LIDAR system has been developed which is capable of measuring temperature and water vapour mixing ratio profiles within the first 2 km of the troposphere, both by day and night. These data are used to determine the radio refractivity profile. The project has been technically demanding, with many equipment issues to resolve, primarily due to the need for high laser power to enable daytime measurements. The technique provides benefits over the use of radiosondes in being able to make continuous measurements, over periods of several hours.

## References

[1] B.R. Bean and E.J. Dutton, "Radio Meteorology", NBS Monograph 92, US Department of Commerce, p.7, 1965.
[2] M.P.M. Hall, L.W. Barclay and M.T. Hewitt, "Propagation of radiowaves", Institution of Electrical Engineers, pp. 105-119, London, 1996.
[3] D.N. Whiteman, S.H. Melfi and R.A. Ferrare, *Appl. Opt.*, 31(16), 3068-3082, 1992.
[4] G. Vaughan et al., *Q.J.R. Meteorol. Soc.*, 114, 1471-1484, 1988.
[5] V. Sherlock, A. Hauchecorne and J. Lenoble, *Appl. Opt.*, 38(27), 5816-5837, 1999.
[6] A. Ansmann et. al., *Appl. Phys.*, B55, 18-28, 1992.
[7] S.E. Bisson, J.E.M. Goldsmith and M.G. Mitchell, *Appl. Opt.*, 38(9), 1841-1849, 1999.
[8] D.D. Turner et al., *J. Atmos. Oceanic Technol.*, 19, 37-50, 2002.
[9] G. Vaughan et al., *Appl. Opt.*, 32(15), 2758-2764, 1993.
[10] A. Behrendt and J. Reichardt, *Appl. Opt.*, 39(9), 1372-1378, 2000.
[11] A.J. Gibson, "Simulation of high resolution Raman spectra for LIDAR applications", NRPP Research Note 156, Radiocommunications Agency, 1995.

 